Electronics Shielding and Reliability Design Tools

J.W. Wilson[1], P.M. O'Neill[2], T.A. Zang[1], J.E. Pandolf[1],
Steven L. Koontz[2], P. Boeder[3], B. Reddell[3], C. Pankop[3]
[1]NASA Langley Research Center
[2]NASA Johnson Space Center
[3]The Boeing Company
POC: john.w.wilson@nasa.gov

Abstract

It is well known that electronics placement in large-scale human-rated systems provides opportunity to optimize electronics shielding through materials choice and geometric arrangement. For example, several hundred single event upsets (SEUs) occur within the Shuttle avionic computers during a typical mission. An order of magnitude larger SEU rate would occur without careful placement in the Shuttle design. These results used basic physics models (linear energy transfer (LET), track structure, Auger recombination) combined with limited SEU cross section measurements allowing accurate evaluation of target fragment contributions to Shuttle avionics memory upsets. Electronics shielding design on human-rated systems provides opportunity to minimize radiation impact on critical and non-critical electronic systems. Implementation of shielding design tools requires adequate methods for evaluation of design layouts, guiding qualification testing, and an adequate follow-up on final design evaluation including results from a systems/device testing program tailored to meet design requirements.

Introduction

Improved spacecraft shield design requires early entry of radiation constraints into the design process to maximize performance and minimize costs. As a result, we have been investigating computational procedures to allow shield analysis starting with preliminary design concepts through high-fidelity final design models (Wilson et al. 2003). Of particular importance is the need to implement probabilistic models to account for design uncertainties (Wilson et al. 2004) in the context of optimal design processes (Qualls et al. 2003). These requirements need supporting tools with high computational efficiency to enable appropriate design methods. Only the HZETRN code of the National Aeronautical and Space Administration (NASA) has so far been identified for this purpose within the NASA STD-3000 (2005) document. As a result, Wilson et al. (2005) have prepared a review of past HZETRN code development, verification, and validation. In addition, there has been renewed interest in incremental improvements of the HZETRN code to assure the timely development of improved efficient computational procedures to support new design processes.

As NASA's newly defined technology development spirals are now progressing, there is a need to provide design tools for the early spiral processes for return to and further exploration of the moon (development of a Crew Exploration Vehicle, CEV) in preparation for going on to Mars. Provision of such design methods is critical to the use of low-cost commercial-off-the-shelf (COTS) electronic devices and systems with their, often, high radiation sensitivity and manufacture variability. A similar shield design tool development activity for human protection under the Constellation Program already includes evaluation of the natural and induced environments mapped throughout the modeled vehicle to assure astronaut safety, thus providing most of the software framework required for electronics shield design and evaluation including charge buildup in dielectric components. Preliminary software has likewise been prepared for JPL's Team X multidisciplinary design environment. The present project would prepare modified software tools for use in electronics shield design with appropriate NASA mandated verification and validation processes using Shuttle and International Space Station (ISS) flight data. This provides a well-validated tool for use in Crew Exploration Vehicle design and first flight in low Earth orbit (LEO) validation. User-friendly design engineering interfaces for use in multidisciplinary design processes allowing optimization and reliability design methods supported by high-speed computational procedures will be discussed. Such tools will be of utmost important for electronics placement in these large-scale human rated systems.

Design Tool Development

A schematic overview of the design tool functionality being developed under the Constellation Program is shown in Fig. 1. Spacecraft shield geometry specification is a central part of model development but the response of sensitive systems (such as human tissue models) is an integral part of the design process. The analysis/interface tools imply interaction with other non-radiation related tools shown as the bottom tier of the figure. Present interest in integration of flight data

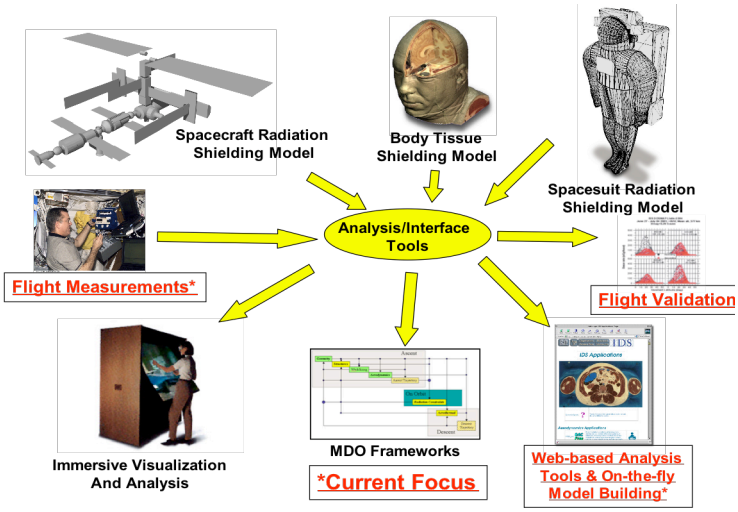

Fig. 1. Schematic overview of radiation analysis and design tools.

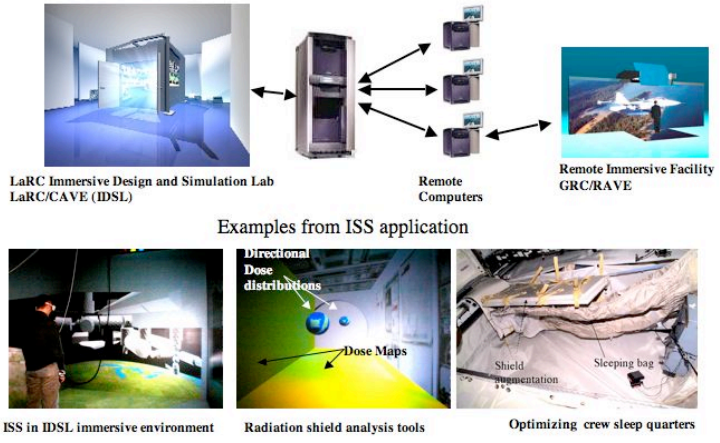

Fig. 2. Collaborative immersive virtual reality frameworks for radiation analysis.

is shown on the left of the figure, interfacing with ISS models and detector response functions, and comparing with flight measurements to validate the galactic cosmic ray (GCR) and South Atlantic Anomaly (SAA) analysis tool functionality. Application focus is on web-based analysis tools with on-the-fly model building to be made available to Constellation development teams.

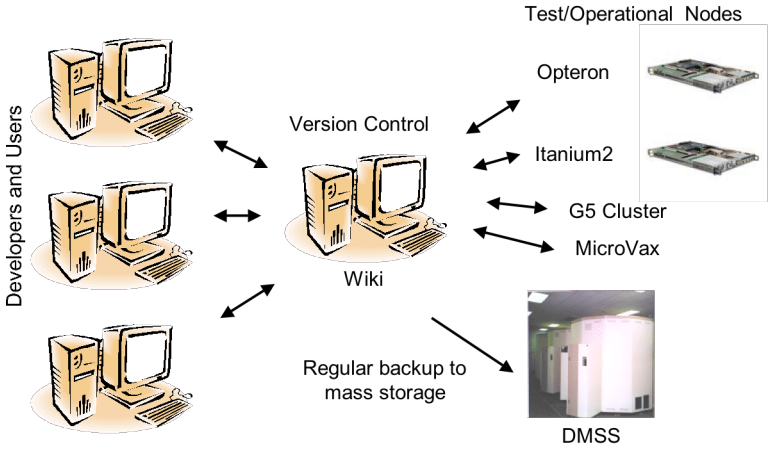

Fig. 3. Current development environment for web-based tool applications.

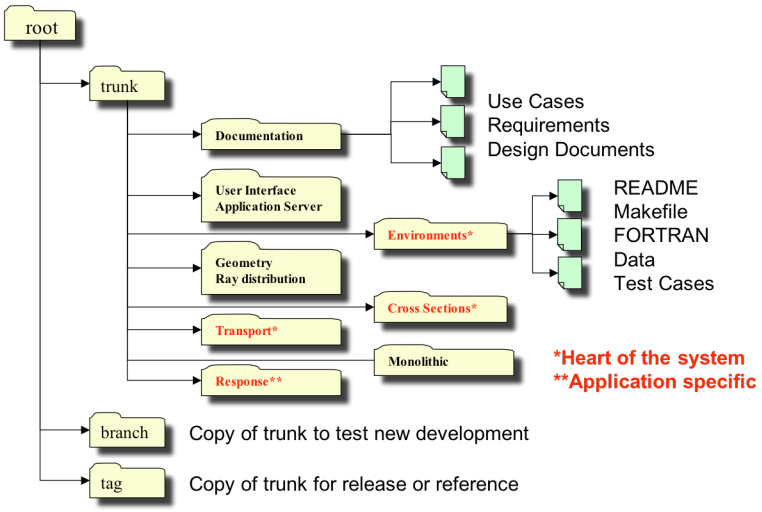

Fig. 4. System version control repository structure.

An example of a prior application focus on immersive reality visualization methods of shield evaluation is shown in Fig. 2, in which an ISS application to study inherent shield functionality in preparation of placement of shield augmentation in crew sleep quarters was made and lead to autonomous optimization methods for placement of augmentation materials (Qualls et al. 2003). The autonomous optimization methods are well-suited for the Multidiscplinary Optimization (MDO) procedures in the bottom tier of Fig. 1. Clearly, such methods require an infrastructure of high-performance computational technology and efficient computational procedures. Consequently, the dose maps used to locate radiation hot spots within the spacecraft design as shown in Fig. 2 can be generated in a few minutes and directional dose patterns used to examine the shielding around an exposure location can be generated at arbitrary locations in several seconds (VerHage et al. 2002). Full collaborative capability was demonstrated for the ISS simulation between the Langley Research Center CAVE and the Glenn Research Center RAVE facilities using the ISS simulation models and avatars representing members in the distal facility.

The development environment for the web-based applications is shown in Fig. 3. The user/developer interface is handled by a Wiki through which process functionality is controlled for the user and version control is implemented for the developers. The

functionality and testing is facilitated by interface with a vast array of computational infrastructure for development, testing, and applications as noted in the figure. The entire system is regularly backed up through a mass storage device (DMSS) housed at the Langley Research Center.

Version control is part of the verification and validation process mandated as NASA standard practice for engineering software development (NASA Procedure Requirement NPR 7150.2). It also coordinates the work of several people working on different pieces or versions of the same code or codes. It also facilitates automated testing of components and integrated software systems for verification and validation. It allows a project-wide undo button back to a specific date to interrogate functionality before a specific feature was added or modified allowing debugging of code error and verification. It also supports release of special versions (e.g., a version for the recent Exploration Systems Architecture Study--ESAS) with continued updating of original versions. It functions as a project time machine to track new methods and retrace to old methods for comparisons and verification.

Version control is implemented in the context of a repository structure shown in Fig. 4. The heart of design processes lies in environmental models, transport methods, and supporting cross section datasets. Response functions depend on the material being protected and human geometry and response functions are those currently modeled in the system along with detector response functions used for flight validation. The monolithic portion of the chart is the contact point with final research codes to be transitioned into the engineering framework providing the interface with the research groups developing new verified and validated methodologies (Wilson et al. 2006a, 2006b).

Enabling Technology

The development of such a system is enabled by high-performance computational methods based on direct solution of the Boltzmann transport equation. This multidimensional system of partial integral-differential equations defined over three position variables and three motion variables describe all of the processes by which ionizing radiation (in this context radiation refers to waves and energetic particles) interact with bulk materials including molecular, atomic, and nuclear processes. The Boltzmann equation describes the radiation flux of type j particles $\phi_j(\boldsymbol{x},\boldsymbol{\Omega},E)$ (including photons) as

$$\boldsymbol{\Omega}\bullet\boldsymbol{\nabla}\phi_j(\boldsymbol{x},\boldsymbol{\Omega},E) =$$

$$\sum_k \int \sigma_{jk}(\boldsymbol{\Omega},\boldsymbol{\Omega}',E,E')\,\phi_k(\boldsymbol{x},\boldsymbol{\Omega}',E')\,d\boldsymbol{\Omega}'\,dE' - \sigma_j(E)\,\phi_j(\boldsymbol{x},\boldsymbol{\Omega},E)$$

where $\sigma_j(E)$ and $\sigma_{jk}(\boldsymbol{\Omega},\boldsymbol{\Omega}',E,E')$ are the shield media macroscopic cross sections and incoming flux is specified at the material boundary. The $\sigma_{jk}(\boldsymbol{\Omega},\boldsymbol{\Omega}',E,E')$ represent all those processes by which type k particles moving in direction $\boldsymbol{\Omega}'$ with energy E' produce type j particles in direction $\boldsymbol{\Omega}$ with energy

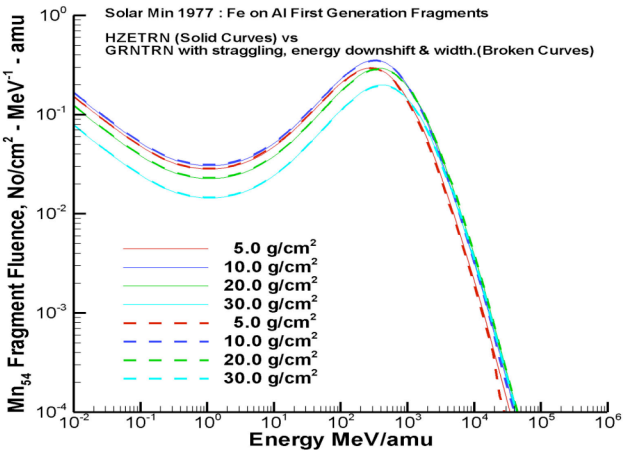

Fig. 5. Verification of marching procedure (HZETRN) by comparison with analytic approximation (GRNTRN).

E (including decay processes). The solution methods are based on three levels of physical perturbation approximations based on molecular/ atomic processes, nuclear elastic scattering, and nuclear reactive processes where process cross sections and energy transfers differ by many orders of magnitude. The resulting equations are simplified by asymptotic expansions for which the first asymptotic terms are highly directed forward with a simplified Boltzmann description in terms of a Volterra equation that can be solved by marching procedures or Neumann series expansion. The broad angle corrections are treated in perturbation series to first order with higher-order neutron diffusion terms evaluated using numerical procedures (Wilson et al. 2002).

Verification of the combination of analytical and numerical procedures used in implementing the Boltzmann equation is through two processes. All of the ions with charge greater than 2 are produced in the near forward direction and the first order asymptotic expansion is highly accurate for broad beams and/or spectra. The corresponding Volterra equation is solved by both analytical methods using the Neumann series (GRNTRN) and marching procedures (HZETRN). Verification using the Mn-54 flux evaluated with the two methods is shown for Fe ions at 1977 GCR solar minimum conditions incident on aluminum of varying thickness as shown in Fig. 5 (Tweed et al. 2006). It is clear that the two solution methods are hardly distinguishable. A second verification method is to compare the marching procedure (HZETRN) with a full 3D Monte Carlo simulation (HETC). Such a comparison for the calculation of dose equivalent in 30-cm of water shielded by 20 g/cm^2 of iron is shown in Fig. 6. A major difference is in the computation time of the two codes. The HZETRN values are ready in about 3 seconds for both the solar particle event and the full 1977 GCR spectra evaluated

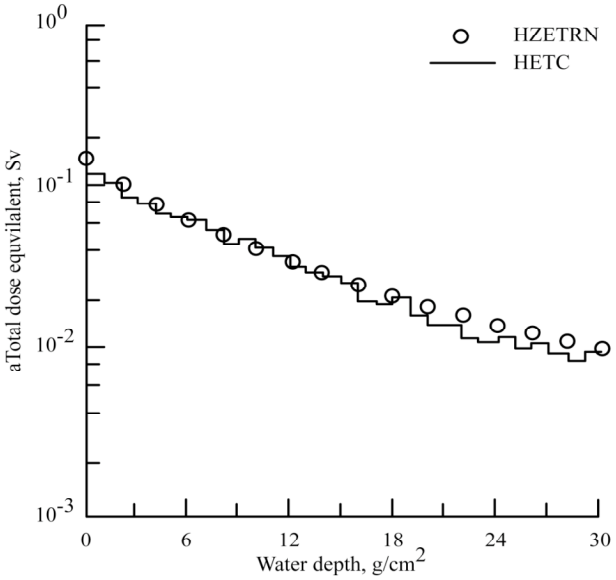

(b) Iron shield on water. 20 g/cm^2 Fe; 30 g/cm^2 water.

Fig. 6. Verification using dose equivalent evaluation with HZETRN and HETC in 30-cm water shielded by iron at 20 g/cm^2 from the Webber model solar particle event.

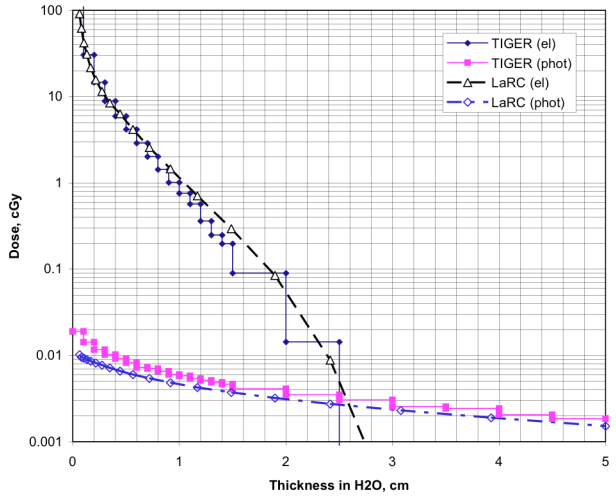

Fig. 7. Verification using dose in water for incident electrons according to LaRC ELTRN and the Air Force TIGER code.

in parallel using a MicroVax Alpha machine while the HETC requires tens of hours for the solar particle event alone while the GCR spectrum is expected to require orders of magnitude more computational time. The Boltzmann equation can also be solved for an incoming electron flux present at the material boundary. Again, high-performance solution methods are developed and verified using Monte Carlo comparisons. The dose in water from penetrating electrons and secondary photons is shown in Fig. 7 for the Langley derived ELTRN code and the TIGER Monte Carlo code. Again, there are many orders of magnitude differences in time required to get results with TIGER taking tens of hours to complete.

Validation follows two tracks. First is the validation of basic computational procedures and databases (molecular/atomic and nuclear) using well-defined particle beams and detailed experimental characterization of the resulting fields produced in materials. The laboratory setup is shown schematically in the upper left corner of Fig. 8. One such implementation at the Brookhaven National Laboratory's Alternating Gradient Synchrotron (AGS) is shown in the lower left corner of the figure. A sample dataset of energy loss spectra behind a graphite-epoxy target measured by the downstream detectors is shown in the right half of Fig. 8 along with an analytic solution of the first asymptotic term of the Boltzmann equation solution as was used also in the verification

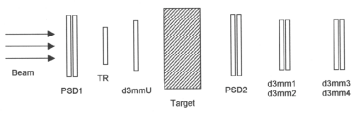

Laboratory test set up

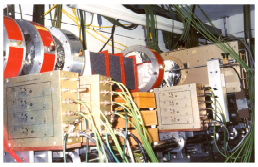

Testing TransHab Wall

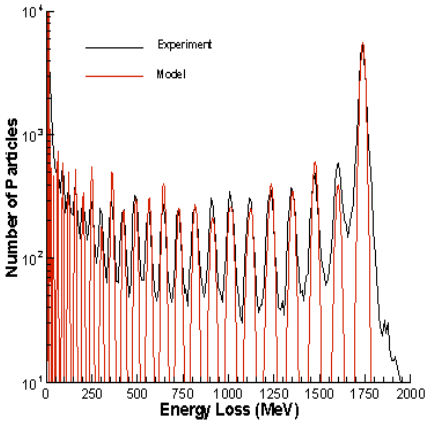

Energy loss spectra behind 10 g/cm^2 graphite epoxy

Fig. 8. Depiction of the validation process using laboratory ion beams at the Brookhaven National Laboratory.

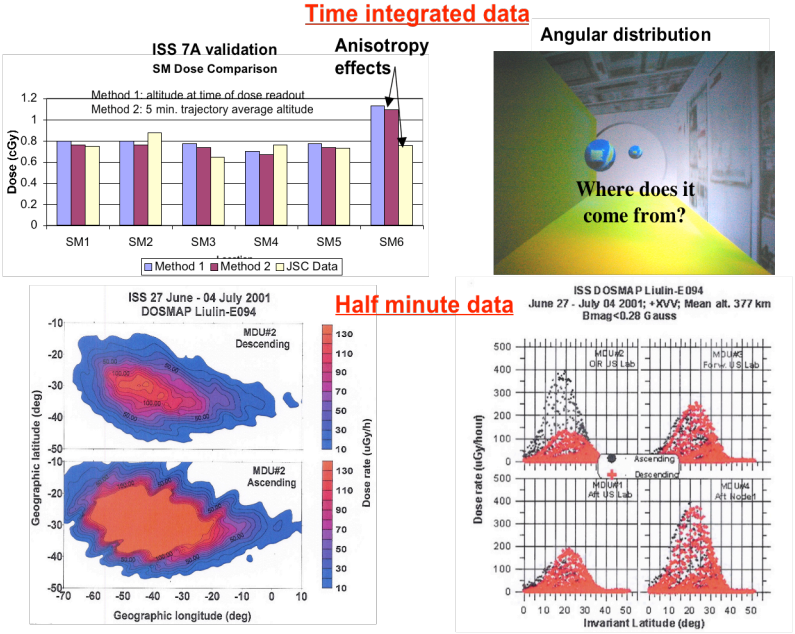

Fig. 9. Examples of flight data used in prior analysis of LEO environments and ISS shielding. Note the extremely intense regions of the trapped particles in the SAA are anisotropic as seen by the ascending/descending differences in the lower graphs.

process in Fig. 5. Such validation requires a detailed understanding of the response of the detector systems. In this comparison, the large peak to the right is from the penetrating iron ions and iron produced fragments. The width of this peak is determined by fluctuations in the molecular/atomic collision processes. The next peak to the left is due to manganese fragments produced in the breakup of the iron ions in nuclear collisions and the width of this peak is determined by specific nuclear dynamics in the collision process. Remaining peaks to the left are fragments produced with lesser charge.

The second validation method is through flight measurements involving specific flight platforms. Unlike the laboratory validation where the radiation source and material geometry is simple and well understood, the flight validation is often limited by uncertainty in environmental models, uncertainty in material arrangement and properties of complicated spacecraft, and uncertainty in detector response. In order to effectively use flight measurements, one must provide detailed analysis to isolate the cause of differences in flight data and computational models. Some examples of this process are shown in Fig. 9. Two types of datasets are available: time integrated and rate data shown in the upper and lower tiers of Fig. 9 respectively. The time integrated response registered in thermo-luminescent detectors located at standard locations within the ISS Service Module were generally in good agreement with computational results from the omni-directional radiation models available at the time of analysis as seen in the upper left of Fig. 9. Detector SM-6 located in a thin pressure adapter section however was out of line with the remaining measurements (Hugger et al. 2003). The directional dependence of the trapped radiation in passage through the South Atlantic Anomaly was examined in an immersive virtual reality environment as seen in the upper right of the figure and subsequently modeled for the simulations giving a satisfactory explanation of the differences in the SM-6 measurements. The original omni-directional assumption allowed overestimation of penetration of the thin pressure adaptor wall where in reality little of the trapped particles enter this way but are intersected by thicker portions of the Service Module when anisotropies are better accounted for in the models (Hugger et al. 2003). Anisotropies are now a general feature of current LEO environmental models (Wilson et al. 2006a).

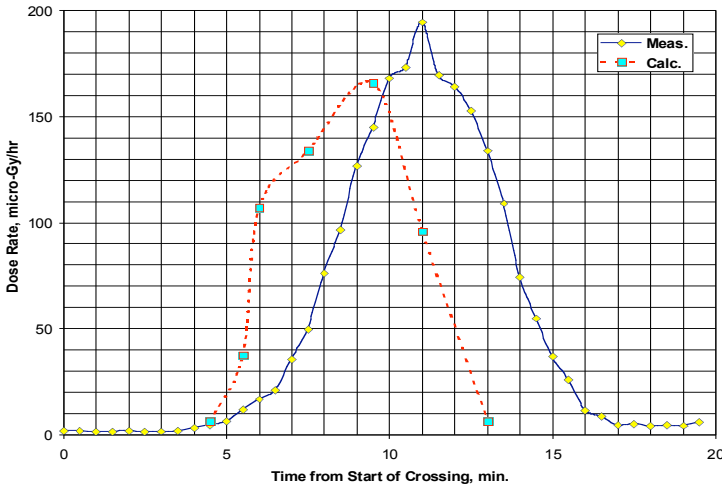

Fig. 10. Dose rate measured on a single descending passage through the heart of the SAA compared to computational model results.

An example set of rate data measured by the Liulin-094 detector system in the US Laboratory and Node 1 of ISS during 27 June-4 July 2001 (Dachev et al. 2006) is shown in the lower tier of Fig. 9. One advantage of such a measurement is the clear separation between the trapped component and the GCR background component. As seen on the

lower left, there are great differences in dose rate for passages through the SAA depending on location of the ascending and descending node lines. These differences in ascending and descending passages are even better quantified when correlated with invariant latitude (a geomagnetic related coordinate). A single pass through the SAA along a descending phase trajectory is shown in Fig. 10 in comparison to the current modeled values (Wilson et al. 2007).

A critical experiment was performed by Badhwar et al. (1995) using the PHIDE instrument examining secondary particle spectra produced by GCR at high latitudes in Shuttle orbit. In this experiment, the Shuttle geometry and materials as well as the GCR environment with the geomagnetic cutoff are well understood. The detector was a well-calibrated particle telescope so that the uncertainties usually associated with flight experiments were minimized in this study. The measured and calculated secondary protons produced by GCR penetration of the Shuttle hull are shown in Fig. 11. It is clear that the secondary proton production and transport processes in the current computational model (HZETRN) is accurately described (Shinn et al. 1998). Other important secondary particles are the neutrons. Although some neutrons present at LEO are the albedo neutrons produced in the Earth's atmosphere as a result of impact of the GCR, most neutrons in a large human-rated spacecraft are produced in the surrounding spacecraft structure.

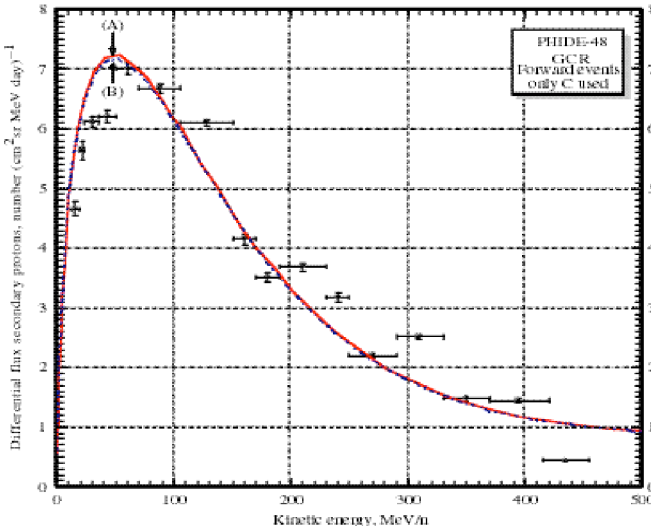

Fig. 11. Comparison of measured secondary proton data with error bars produced by GCR in the Shuttle hull with computational models.

Neutrons have been studied on space station Mir and ISS using a variety of techniques as shown in Fig. 12. Unlike the particle telescope used by Badhwar for charged components, there is considerable uncertainty in most space neutron measurements. Monte Carlo calculations of neutrons produced by GCR protons calculated by Getselev et al. (2004) are also shown for simplified shield geometry. Note the multiple charged GCR ion contributions as well as the trapped radiation contributions to the neutron fields within Mir and ISS are ignored in the Monte

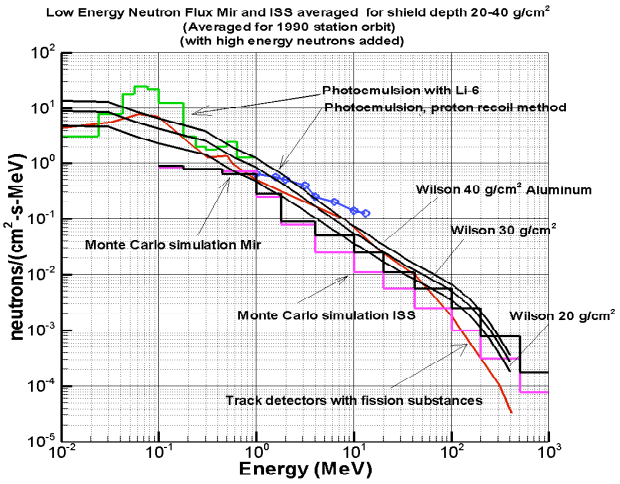

Fig. 12. Comparison of neutron spectral measurements on Mir and ISS with Monte Carlo and current models.

Carlo values. The distribution of shielding about the detector is not clearly specified. Guided by the comment that the shielding about the detectors varied from 20-40 g/cm^2 we have evaluated the LEO neutron spectra from all environmental components (GCR, trapped protons, albedo neutrons) in aluminum spheres of thicknesses of 20, 30, and 40 g/cm^2 for comparison to measured results as shown in the figure. The preliminary results of recent computational procedures are encouraging but require further study.

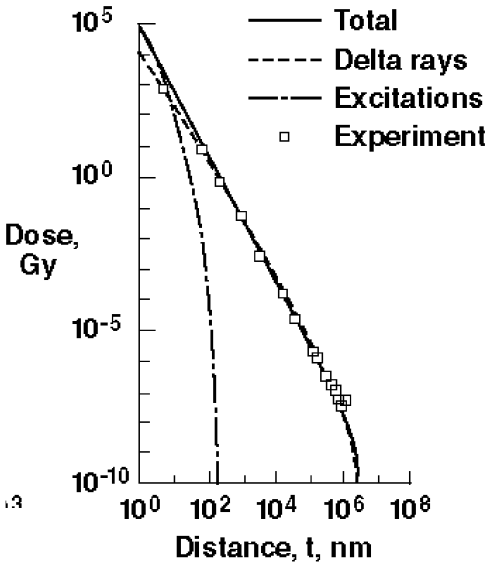

Fig. 13. Physics based radial energy deposition model and experimental validation.

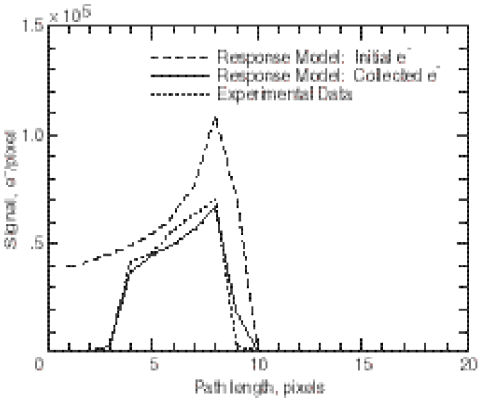

Fig. 14. Auger recombination effects in CCD device response to a 2.4 MeV proton.

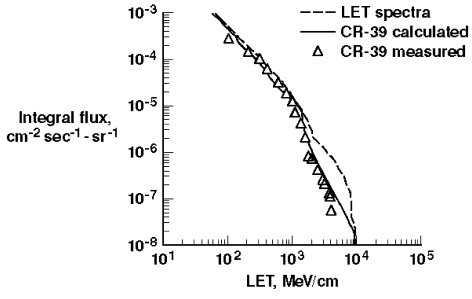

Fig. 15. CR-39 measured LET spectra compared to modeled CR-39 response and true LET spectrum.

Electronic Response Models

The computational models with verification and validation processes discussed to this point are common to any shield design problem whether it is for protecting astronauts, various materials, or electronic devices. Specific shield design application is through the specification of responses and mission design requirements. Similar to the case of human protection, response functions are driven by basic physical processes through which energy is handed over to sensitive materials or tissues. There are two main processes by which energy is transferred to sensitive materials, first is the transfer to the orbital electrons leading to direct ionization and the second is the displacement of atoms from well ordered lattice sites on which the device function depends.

The transfer of energy from a passing energetic ion to orbital electrons provides a local electron flux propagating from the ion path into the material producing additional ionization and excitation. Aside from the addition of dose to the bulk material, these electrons produce a current if local electric fields are present and initiate chemical change in materials through ionization and excitation processes. Such energy deposition events are studied in low-pressure gas filled proportional counters and correlated with theory as shown in Fig. 13. The high-energy density in electronic devices provide high

electron-hole pair densities near the central track of the ion path resulting in Auger recombination effects limiting the response of electronic devices depending on the exact nature of the energy deposit and the charge collection time of the device. Such effects are seen in a CCD array (Charge Coupled Device) exposed to 2.4 MeV protons as shown in Fig. 14. The total linear energy transfer (LET) from the ionization per distance traveled related to the initial electron density within a pixel is shown in the figure. The collected electrons are limited by Auger recombination as also shown in the figure and are in good agreement with experimental measurements. Recombination chemistry is also affected by the free radical density that similarly varies as a function of distance from the ion path. These effects are seen in the chemically etched ion tracks where etched track radii assumed proportional to the LET in CR-39 nuclear track detectors as shown in Fig. 15. The experimental CR-39 LET distribution with its limitations from recombination chemistry and the modeled CR-39 response are shown with the modeled LET distribution where the main differences are for low-energy target fragmentation event contributions which register more poorly in the CR-39 detectors.

Table 1. Validation of Shuttle shield model and memory SEU model (SEU/computer-day).

Mission	Flight data	Model
STS-51	2.13	1.52
STS-56	6.05	5.85

Auger recombination effects for low-energy target fragments within electronic devices is demonstrated in the Shuttle computers (Shinn et al. 1995) with results of SEU rate (SEU/computer-day) for STS-51 at low orbit inclination and STS-56 at high inclination shown in Table 1. The SEU from target fragments produced mainly by protons and neutrons colliding with the Si nuclei of the memory chips is grossly overestimated if the Auger processes are ignored (Shinn et al. 1995). With Auger recombination, reasonable agreement is obtained with computational models as seen in the Table 1.

Many materials depend on the high-quality ordering of lattices to maintain their desirable physical properties such as optical properties and electronic properties. Defects through lattice displacements in collisions with environmental radiation components degrade material performance. Again basic physics models are the starting point of such material effects. The lattice displacement dynamic variables are displayed for gallium arsenide (GaAs) based materials in Fig. 16 as the total displacement cross sections, $\sigma_D(E)$ in units of barns (1 barn = 10^{-24} cm^2) for protons

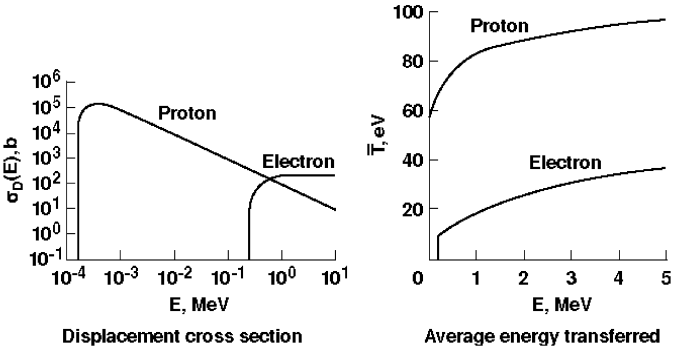

Fig. 16. Physics based lattice displacement models used in electronics modeling.

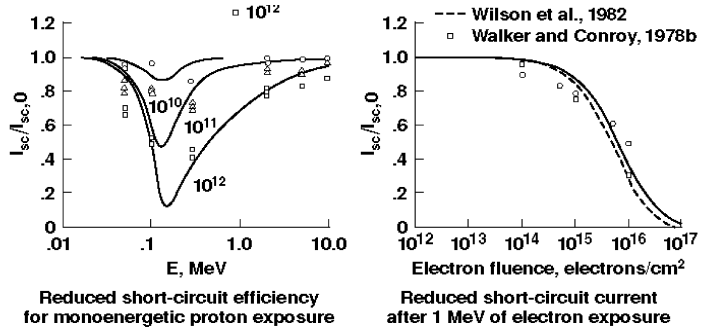

Fig. 17. Physics based short circuit response model of GaAs shallow junction solar cells.

and electrons of energy E MeV. Also shown is the average energy transfer to the initially displaced atom in units of eV and used to estimate the total number of displacements per unit volume of material. The effects of thresholds due to lattice binding are clearly displayed in these displacement functions. These functions were applied to analysis of Langley developed GaAs shallow junction solar cell short circuit current experiments using low-energy proton and electron beams as shown in Fig. 17. On the basis of these studies, Wilson et al. (1982) predicted that the equivalent 1 MeV electron damage coefficient, D(E), would be dependent on the level of reduction of the short circuit current as shown in Fig. 18 for 20 and 80 percent short circuit reduction levels. Experimental confirmation of these results was reported by Anspaugh and Downing (1984). It is clear that physics based response models are useful approaches for understanding the response of materials to radiation insult. From these models, one can design a testing program to simulate the processes affecting the material as a combination of LET, dose, and displacement damage effects.

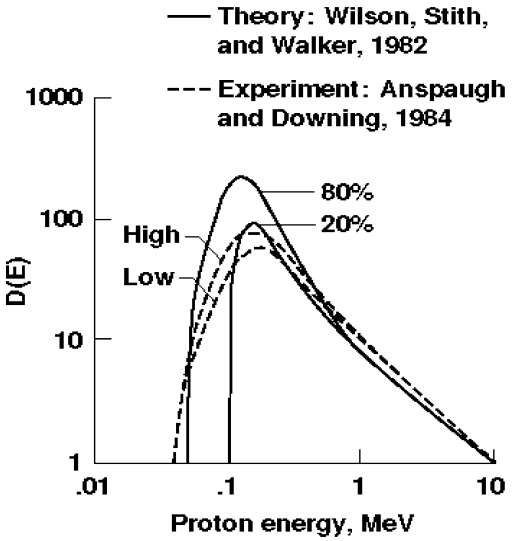

Fig. 18. Equivalent 1 MeV electron fluence ratio as a function of proton energy.

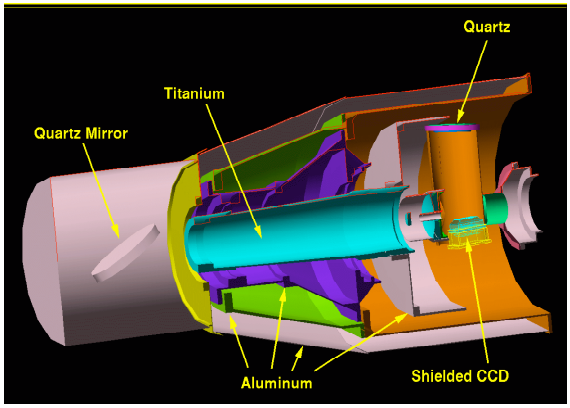

Fig. 19. SAGE-III shielding model used in CCD shield design.

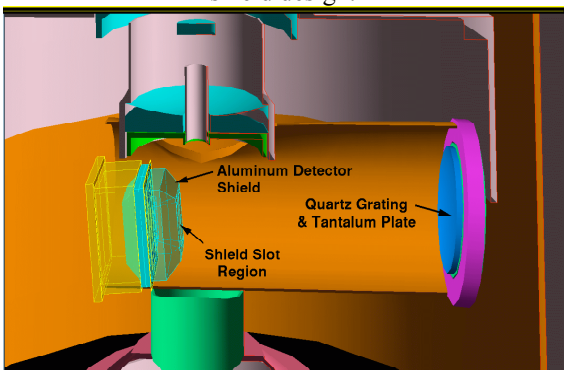

Fig. 20. Final SAGE-III detector shield with aluminum alloy.

Spacecraft Analysis Method

It is instructive to go through a specific design process to see how the above processes are brought together to accomplish an end design product. The SAGE-III instrument (Fig. 19) samples light from the Earth's atmosphere and passes it down an optical bench to a quartz grating which is focused on a CCD array to quantify the optical frequency distribution. The CCD is sensitive to displacement damage in its active layers. It was anticipated that energetic trapped electrons would be a major limiting factor in the performance of the device and a tantalum shield was planned because of the efficient multiple scattering limiting electron penetration. A detailed shielding model was developed as shown in Fig. 19 for the analysis. Although the electron

induced displacements were indeed the major contributor to CCD degradation as expected, it was neutrons produced in the tantalum shield that also contributed to driving the CCD beyond requirements. An aluminum detector shield was designed to adequately limit electron penetration and reduce the neutron component as shown in Fig. 20.

Concluding Remarks

The Constellation Program requires verified/validated/standardized analysis, design, and testing procedures for quality assurance of future hardware. This involves the improvement and validation of environmental models and computational procedures for Constellation design teams. From a hardware perspective, environment and shielding design tools will be coupled to hardware specific damage functions of which the first level is evaluation of basic physics models for total ionization, displacement damage, and linear energy transfer spectra. These basic quantities then couple to specific device response models with shielding analysis and shield materials optimization. The output of such analysis would include design specific testing protocols for qualification that assures the proper mix of basic physical processes (dose, dose rate, displacement damage, and LET spectral contributions) to be matched to available accelerator capabilities (electrons, protons, high energy heavy ions). The design tool software can then be run in a design validation to qualify with test-flight data in low Earth orbit for design prediction validation mode for Lunar and Mars mission design validation. Developing design tools plays a central role in the above processes and at minimum added costs when leveraged out of the human protection program.

References

Anspaugh, B.E., Downing, R.G., *Radiation effects in Silicon and Gallium Arsenide solar cells using isotropic and normal incident radiation.* NASA CR-174007, 1984.

Badhwar, G.D., Patel, J.U., Cuccinotta, F.A., Wilson, J.W., Measurements of the secondary particle energy spectra in the Space Shuttle. *Rad. Meas*. **24**:129–138; 1995.

Dachev, T., Atwell, W. Semones, E.; Tomov, B., Reddell, B., ISS Observations of SAA radiation distribution by Liulin-E094 instrument. *Adv. Space Res*. **37**: 1672-1677; 2006.

Getselev, I. et al., Absorbed dose of secondary neutrons from galactic cosmic rays inside international space station. *Adv. Space Res.* **34**: 1429-32; 2004.

Hugger, C.P. et al., *Preliminary validation of an ISS shielding model*. Space 2003 Conference. AIAA 2003-6220, 2003.

NASA, *STD-3000, Vol. VIII, Human-Systems Integration Standards, Crew Exploration Vehicle Launch Segment.* http://www.exploration.nasa.gov/acquisition/cev_procurement.html

Qualls, G.D., Wilson, J.W., Cucinotta, F.A., Nealy, J.E., Hugger, C.P., Atwell, W., Shavers, M.R., *International Space Station radiation shield augmentation optimization*. Space 2003 Conference AIAA 2003-6222, 2003.

Shinn, J. L., Cucinotta, F. A., Wilson, J. W., Badhwar, G. D., O'Neill, P. M., Badavi, F. F., Effects of target fragmentation on evaluation of LET spectra from space radiation in low-Earth orbit (LEO) environment: Impact on SEU predictions. *IEEE Trans. Nucl. Sci.,* **42**(6): 2017-2025; 1995.

Shinn, J. L., Cucinotta, F. A., Simonsen, L.C., Wilson, J. W., Badavi. F.F., Badhwar, G. D., Miller, J., Zeitlin, C., Heilbonn, L., Tripathi, R. K., Clowdsley, M. S., Heinbockel, J. H., Xapsos, M. A., Validation of a comprehensive space radiation transport code. *IEEE Trans. Nucl. Sci.* **45**(6): 2711-2719; 1998.

Tweed, J., Walker, S.A., Wilson, J.W., Tripathi, R.K., Cucinotta, F.A., Badavi, F.F., *An improved Green's function for HZE ion transport*. SAE ICES 2006-01-2147, 2006.

VerHage, J.E., Sandridge, C.A., Qualls, G.D., Rizzi, S.A., ISS radiation shielding and acoustic simulation using an immersive environment, *Immersive Projection Technology 2002 Symposium*, Orlando, FL, March 24-25, 2002.

Wilson, J.W., Stith, J.J., Walker, G.H., On the validity of equivalent electron fluence for GaAs solar cells. *Sixteenth IEEE Solar Photovoltiac Specialists Conference*, pp. 1439-1440, 1982.

Wilson, J.W. et al. Advances in space radiation shielding codes. *J. Radiat. Res*. **43**: S87-S91; 2002.

Wilson, J.W., Korte, J.J., Sobieski, J., Badavi, F.F., Chokshi, S.M., Martinovic, Z.N., Cerro, J., Qualls, G.D., *Radiation shielding, MDO processes, and single stage to orbit design*. Space 2003 Conference, AIAA 2003-6259, 2003.

Wilson, J.W., Cucinotta, F.A., Schimmerling, W. Emerging radiation health-risk mitigation technologies. *Space Technology Applications & Information Forum,* STAIF-2004, AIP Conference Publications, 2004.

Wilson, J.W., Tripathi, R.K., Mertens, C.J., Blattnig, S.R., Clowdsley, M.S., Cucinotta, F.A., Tweed, J., Heinbockel, J.H., Walker, S.A., Nealy, J.E. *Verification and validation: High charge and energy (HZE) transport codes and future development*. NASA/TP-213784, 2005.

Wilson, J.W., et al., International Space Station: A testbed for experimental and computational dosimetry. *Adv. Space Res*. **37**: 1656-1663; 2006a.

Wilson, J.W., et al., *Standardized radiation shield design method: 2005 HZETRN*. ICES 2006-01-2109, 2006b.

Wilson, et al., Time serial analysis of the induced LEO environments within the ISS 6A. *Adv. Space Res*. In press, 2007.